Multiscale Membrane Models

Liu, Yang

DOI:
10.33612/diss.136221782

Chapter 6

Applying the virtual site hybrid scheme to investigate lipid relaxation dynamics in vesicles

Abstract

Accurate details on the conformational dynamics of lipids inside membranes can be obtained by measuring C–H bond order parameters and spin relaxation rates in experiments. These data can be also reproduced in molecular dynamics simulations with atomistic details. Due to the computational limitations of simulating at the all-atom level, to date, only small lipid bilayer patches have been simulated to this end. The role of curvature on the conformational dynamics has, therefore, remained unexplored, as this requires simulations of curved membrane systems such as vesicles. In this section, we applied the VS hybrid method on DPPC vesicles in which the inner layer is treated in atomistic detail and coupled to a CG outer leaflet. We systematically increased the size of the vesicle, and computed the C-H bond rotational dynamics and compared it to experimental results, confirming the trend of faster dynamics as the radius of curvature increases.

Method

Simulation setup

We have applied the virtual site (VS) hybrid scheme to planar membrane and vesicle as illustrated in Figure 1. The VS hybrid scheme is a multiscale scheme that can concurrently couple a GROMOS based force field and a modified Martini force field in a single membrane simulation, as explained in Chapter 4. To build the VS dual resolution vesicle, we first built a coarse grain (CG) vesicle using the CHARMM-GUI Martini maker[178]. During the equilibration processes, six artificial pores in the vesicle were kept open with constraints to enhance lipid flip-flop and to equilibrate the number of water beads inside and outside the vesicle[179]. After equilibration, the vesicle was closed by healing the water pores by switching off the restraints. CG water inside the vesicle and the inner leaflets were then mapped into all-atom (AA) resolution with the backmapping software tool backward[128]. Water permeation through the membrane is restrained.

The details of this setup can be found in Chapter 4. For reference, also a planar DPPC membrane (200 lipids per membrane) was simulated.

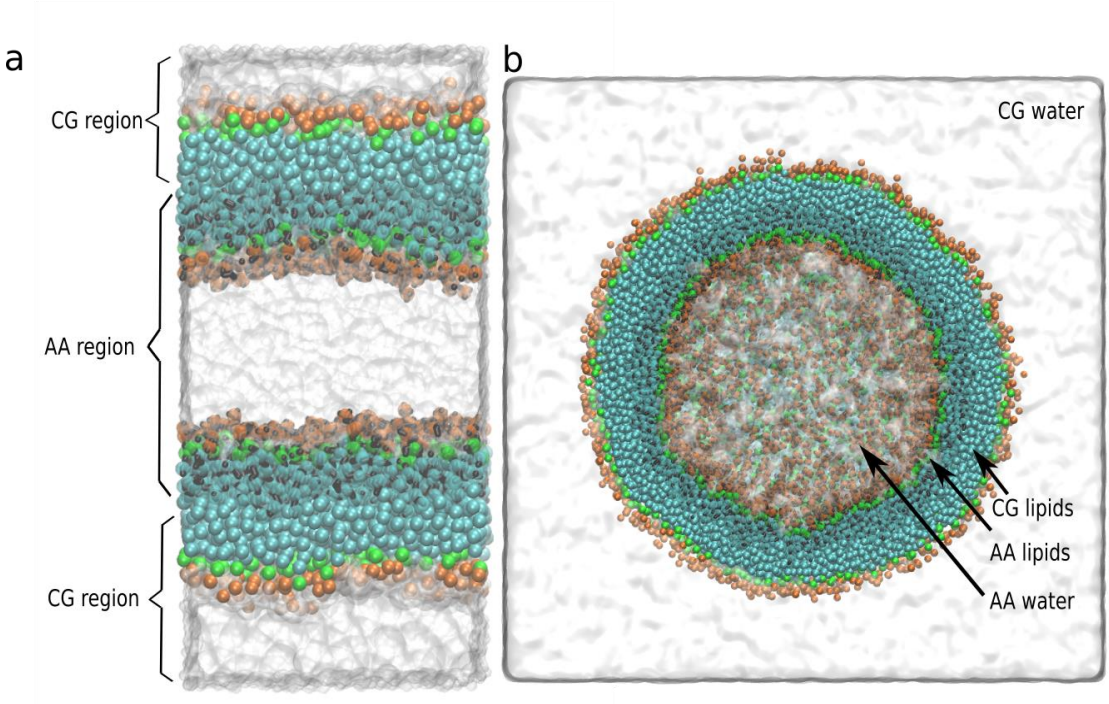

Figure 1. Virtual site hybrid membrane setups. (a) and (b) represent planar membrane and vesicle, respectively. Lipids in the AA region carry virtual sites. Lipids tail, linker, and head parts are represented by cyan, green, and orange color, respectively. The water is rendered by the white transparent surface.

The simulations were carried out using the GROMACS (2016) software. We used an integration time step of 4 fs. The Verlet cut-off scheme was used for the system and the allowed energy error due to the Verlet buffer is 0.005 kJ/mol/ps per atom. The potential modifiers were used to shift the complete LJ and Coulomb potential value to zero at the cut-off. Electrostatic interactions were treated using PME with a 0.12 nm Fourier grid spacing. The temperature was maintained at 323 K by integrating the equations of motion with the leapfrog stochastic dynamics integrator[181] with inverse friction constant of 1 ps to CG (or VS) particles and 0.1 ps to AA particles. AA lipids, AA water, CG lipids, CG water and VS beads were coupled separately to a thermostat. The pressure was kept at 1 bar independently in the lateral and normal directions with the Berendsen barostat[34] in a semi-isotropic pressure bath ($\boldsymbol{\tau}_p$= 0.5 ps) in the planar membrane, while an isotropic pressure bath was used in the vesicle. The compressibility was 4.6×10^{-6} bar^{-1}. The AA bonds were constrained with the LINCS algorithm, and simple point charge (SPC)

water[182] was constrained using SETTLE[183]. All the simulations were carried out for more than 100 ns.

Analysis

For lipids, the so-called order parameter S_{CH} of the C-H bonds in the lipid tail has been studied, mostly because it is accessible experimentally via ^2H-NMR[203]. It can be defined as

$$S_{CH} = P_2 = \frac{1}{2} < 3cos^2\theta - 1 > \quad (1)$$

where P_2 denotes the second Legendre polynomial, θ is the angle between a C-H bond and bilayer normal, and the angle bracket denotes averaging over time. The second-order autocorrelation function for the reorientation of the C–H chemical bond axis is calculated according to:

$$g(\tau) =< P_2[\mu(t)\cdot\mu(t+\tau)] > \quad (2)$$

where $\mu(t)$ is the unit vector in the direction of C–H chemical bond at time t. This autocorrelation is related to experimental spin relaxation rates through a Fourier transformation at frequency w called spectral density:

$$j(w) = 2\int_0^\infty cos(w\tau)g(\tau)d\tau \quad (3)$$

Typically, there are two timescales during the relaxation processes and thus the auto-correlation function can be divided into the fast and slow motions[204-205]:

$$g(\tau) =< g_f(\tau)g_s(\tau) > \quad (4)$$

Here, $g_f(\tau)$ and $g_s(\tau)$ represent the fast and slow decay, respectively, which corresponds to the lipid rotation within the bilayer plane and diffusion between bilayer regions. In liquid crystalline lipid bilayers, the $g_f(\tau)$ decays to the plateau of S_{CH}^2 within hundreds of nanoseconds, which is used to compute the order parameters in $^2H-NMR\ and\ ^{13}C-NMR$ experiments[204]. Therefore, the rotational auto-correlation function can be used to express the average time to sample all conformations within a bilayer plane. The effective correlation time is defined as:

$$\tau_e := \int_0^\infty \frac{g_f(\tau)-S_{CH}^2}{1-S_{CH}^2}d\tau \quad (5)$$

Larger τ_e means longer time required for the conformational sampling. With this definition, the area between the correlation function and its plateau can be written as $(1-S_{CH}^2)\tau_e$.

To analyze the lipid order at AA resolution, Equation 1 was used directly. The united-atom force field implicitly incorporate the aliphatic H-atoms into the carbons to which they are bound. The coordinates of the H-atoms on the aliphatic carbons are estimated based on the positions of

the neighboring carbons assuming tetrahedral geometry. θ represents the angle between the orientation of the C−H bond vector with respect to the bilayer normal in planar membrane. When the CG order parameter was computed, θ represents the angle between the CG bond of the lipid and the bilayer normal. To compute the vesicle outer and inner radius, we computed the distance between the PO4 CG beads (or virtual sites) of the PC lipids in outer (or inner) leaflets and center of mass of the vesicle. The area per lipid were computed using software called FATSLIM[100]. Since the fluctuations or curvature of membrane may introduce noise, the area per lipid is computed based on neighborhood-averaged coordinates to smooth the fluctuations. The specific explanation and software are freely available on the website http://fatslim.github.io/.

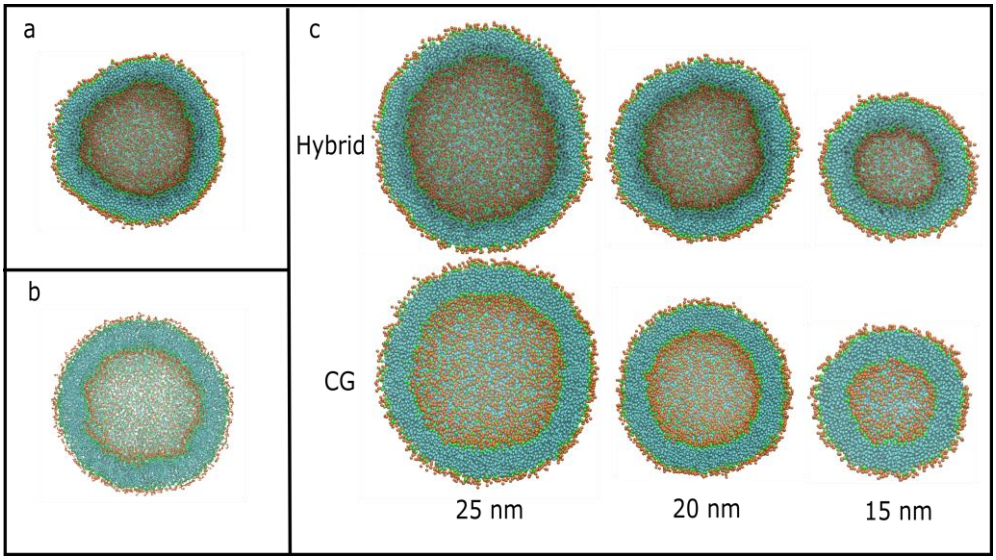

Figure 2. Snapshots of the final configuration of the vesicles. a) and b) represent the hybrid and fully AA vesicles directly backmapped from CG simulations, c) represent the hybrid and CG vesicles with 10% fewer lipids in the inner leaflets. The color scheme is the same as Figure 1. Water is not shown for clarity.

Results

Model validation

To test the model, the VS hybrid scheme was initially applied to a DPPC vesicle with diameter of 20 nm. In our hybrid setup, the inner leaflet together with the interior solvent is modeled in all-atom (AA) detail, using the GROMOS force field, whereas the outer leaflet and exterior solvent are modeled at the coarse-grain (CG) level using the Martini force field. After building and equilibrating a CG vesicle, and converting the inner leaflet to AA resolution, we noted in a 10 ns simulation, that parts of the vesicle form the gel phase that lasts for the whole simulation

(Figure 2a). From the equilibrated hybrid vesicle, we backmapped to a fully AA model and found that also in this case the gel phase persisted during a 5 ns simulation (Figure 2b). This implies that the optimum ratio of lipids in inner and outer leaflets is different between two resolutions.

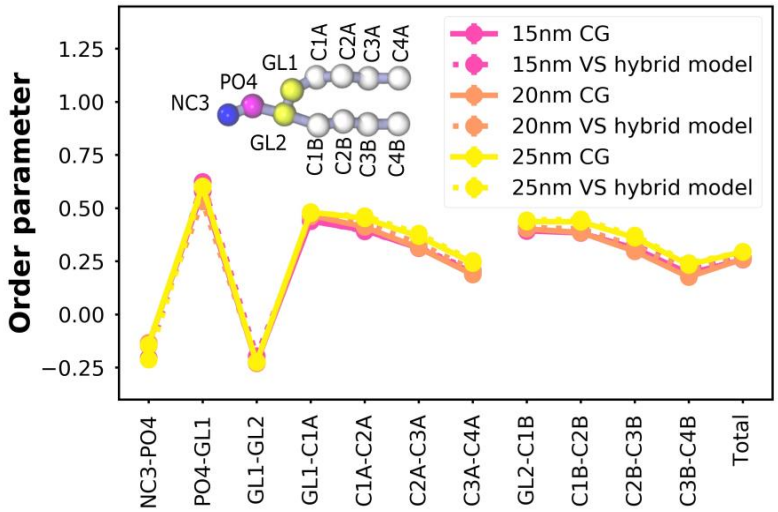

Figure 3. CG order parameter of vesicle outer leaflet lipids. The order parameters are computed based on the bonds connecting CG beads. The error bars are smaller than (or similar to) the size of the data points and the values are listed in Table S1.

Next, in order to solve this imbalance, we deleted 10% lipids from the inner leaflet (the ratio was decided based on trial and error) of the vesicles. We tried to avoid formation of the gel phase and kept the number of deleted lipids as low as possible. The final numbers of lipids in the two leaflets and water molecules/beads inside and outside of the vesicle are listed in Table 1. The VS hybrid scheme was applied to a DPPC vesicle with diameters of 15, 20 and 25 nm. Since it is very expensive to simulate an equilibrated vesicle in atomistic detail, the VS hybrid vesicle was mostly compared against CG simulation. Snapshots of the final configuration of each of the vesicles, after 100 ns simulations, are shown in Figure 2c and reveal that the lipids now keep the liquid crystalline phase. Occasionally, the vesicles are observed to adopt an aspherical shape, but on average they stay spherical. In Table 1, the area per lipid and radius of both inner and outer leaflets of the vesicle are shown. Overall, the hybrid vesicles have structural properties that are close to those of the pure CG ones, although some differences are noticeable such as a thinner membrane in the hybrid scheme. This may, at least in part, be due to the chosen mapping of PO4 beads in the AA leaflet. To further characterize the hybrid vesicles, we computed the CG order parameter of the outer leaflet. The results, presented in Figure 3, show that the order parameter

profiles of the VS hybrid model fit well with the CG vesicle references. This agreement exists in vesicles with different sizes. Taken together, the conformational and structural properties of the VS hybrid vesicles appear reasonable, which is confirmed by the visual inspection (Figure 2c).

Table 1. Membrane properties of DPPC vesicles

System	Diameter (nm)	#Lipid N_{in}/N^{*}_{out}	#Water N_{in}/N^{**}_{out}	Leaflet	Area per lipid (nm^2)	Radius (nm)
CG vesicle	15	356/892	2649/107544	Inner	0.596±0.002	4.1±0.2
				Outer	0.846±0.003	7.7±0.2
VS hybrid vesicle			10596/107544	Inner	0.619±0.002	4.2±0.3
				Outer	0.833±0.002	7.7±0.3
CG vesicle	20	996/1748	10732/174625	Inner	0.558±0.003	6.9±0.8
				Outer	0.804±0.002	10.6±0.8
VS hybrid vesicle			42928/174625	Inner	0.579±0.002	6.8±0.4
				Outer	0.781±0.002	10.4±0.4
CG vesicle	25	1717/ 2774	26131/266286	Inner	0.755±0.003	9.1±0.3
				Outer	0.604±0.002	12.9±0.8
VS hybrid vesicle			104524/266286	Inner	0.742±0.003	9.1±0.3
				Outer	0.607±0.002	12.7±0.3

* Number of lipids in the inner/outer leaflet of the vesicle.

**Number of AA water molecules (or CG water beads) located inside/outside of the vesicle.

***Error margins represent the standard deviation after the system reaches equilibrium. Standard errors are < 0.1%.

Relaxation dynamics of vesicular lipids

In order to investigate the curvature effect on the dynamic properties of the membrane, we simulated the multiscale vesicles with different sizes for more than 100 ns. Only the AA leaflets of the bilayers are used to compute the C-H bond rotational dynamics, since the atomistic details are missing in the CG components. For reference, we also simulated a planar DPPC membrane (radius of curvature ∞). As shown in the inset of Figure 4a, the autocorrelation functions of order parameters for the acyl chains, calculated according to Equation 2, are well converged before the end of the simulations. In Figure 4b, the effective correlation time (Equation 5) is plotted, which

is longer for carbons in the region close to the glycerol group than the ones close to the bilayer center. The magnitude and the overall shape of these profiles are independent of curvature, and similar to those reported by Ollila and Pabst[206] obtained from atomistic simulations of planar membranes. From the data presented in Table 2 and Figure 4b, we can find that the effective correlation time in the planar membrane is shorter than in the vesicles, while the effective correlation time in the different vesicular systems are the same within error bars. The same trend can also be found in Figure 4a, where autocorrelation decays faster in the planar membrane and the rest of the lines overlap with each other. Interestingly, the shorter correlation time of the lipid dynamics in the planar membrane is mostly due to faster dynamics close to the glycerol linker region (Figure 4b). In fact, the terminal groups appear to relax faster inside the vesicles. This difference can be understood considering the negative curvature of the vesicular inner leaflet, leaving relatively less space in the head group region and more space toward the tail ends. Overall, the relaxation time of lipid tails inside the planar membrane is shorter than inside the vesicles, which suggests that the rotational dynamics in the membranes with smaller curvature are faster than the ones with bigger curvature.

It is reported that the order parameters and reorientational correlation times of phospholipid chain are almost identical in small (~35 nm diameter) and large (~95 nm diameter) unilamellar vesicles measured by ^{13}C NMR spin-lattice relaxation rates[207]. The only significant differences in correlation times appear at the carbonyl ends of the acyl chains[207]. It is also found by a pure Martini simulation that the relaxation time of order parameter of both leaflets in a planar membrane is shorter than in a 20 nm diameter vesicle[208]. These results qualitatively agree with our prediction. However, Kel et al. found by 2D IR vibrational echo spectroscopy[209] that the decay of center line slope (ultrafast structural dynamics) of the vesicles (with diameters ranging from 72 nm to 122 nm) becomes faster as the curvature increases. The contradiction between this experimental result and our findings could be caused by the following reasons. The physical meaning of the relaxation time of center line slope may not be entirely identical to what we measured (the relaxation time of the deuterium order parameter) in our simulations. In experiment, the measurement was performed on the vibrational mode of tungsten hexacarbonyl (W(CO)6) in the membrane, however, where exactly the probe sits in the membrane is unclear. In contrast, we directly analyzed the whole acyl lipid group in our simulations. Besides, we only considered the inner leaflet of the vesicle. These

could be the reasons that the decay speed of center line slope in Figure 3 of [209] is about two magnitude faster than the decay speed in our simulations (Figure 4a).

The curvature differences between vesicles with size ranging from 15 nm to 25 nm are rather small and the relaxation times of these systems cannot be distinguished (Table 2). Therefore, in future studies, we will use the Martini force field to simulate the dynamics of vesicles with bigger size and longer simulation time, and probing the properties on both leaflets of the membrane.

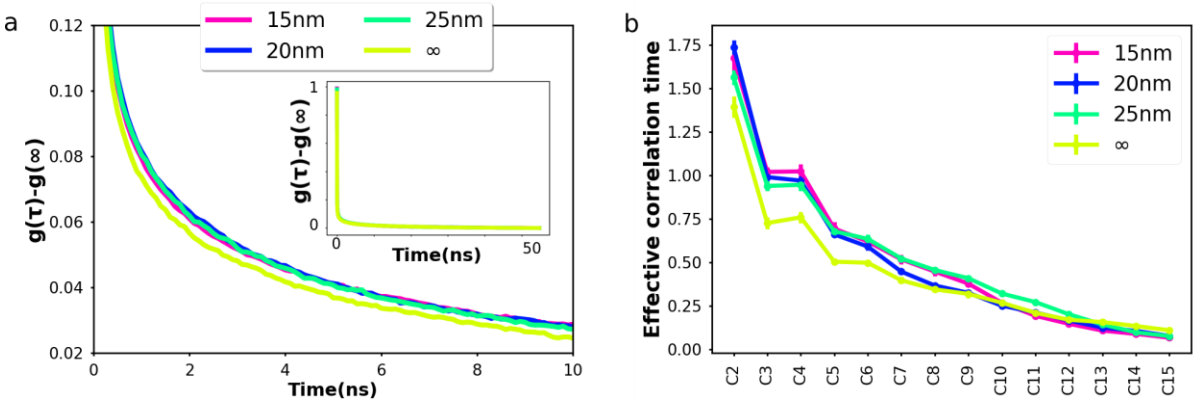

Figure 4. Dynamic properties of lipids in vesicles with different sizes. (a) and (b) show the autocorrelation of order parameters as a function of time (Equation 2) and the effective correlation time of carbons in the fatty acid tails (Equation 5), respectively. The inset in (a) is the entire plot of the autocorrelation reaching more than 100 ns. ∞ denotes the planar membrane.

Table 2. The averaged effective correlation time τ_e (ns)

Size of vesicle	∞	25 nm	20 nm	15 nm
τ_e	0.43 ± 0.02*	0.52 ± 0.02	0.50 ± 0.02	0.52 ± 0.02

* All the data are randomly divided into five groups and the τ_e is computed based on the averaged curve within each group. The standard error of the τ_e of the five groups is used as the error margin.

Supplemental Information

Table S1. CG order parameter of vesicles with different sizes and resolutions

Order parameter	15 nm CG vesicle	15 nm VS hybrid vesicle	20 nm CG vesicle	20 nm VS hybrid vesicle	25 nm CG vesicle	25 nm VS hybrid vesicle
NC3-PO4	-0.14±0.03	-0.20±0.03	-0.14±0.03	-0.13±0.03	-0.14±0.03	-0.21±0.03
PO4-GL1	0.57±0.03	0.62±0.03	0.59±0.03	0.53±0.03	0.60±0.03	0.59±0.03
GL1-GL2	-0.22±0.02	-0.19±0.02	-0.23±0.02	-0.22±0.03	-0.22±0.02	-0.22±0.02
GL1-C1A	0.43±0.03	0.44±0.03	0.46±0.03	0.46±0.02	0.48±0.03	0.47±0.03
C1A-C2A	0.39±0.02	0.39±0.03	0.41±0.03	0.42±0.03	0.45±0.03	0.46±0.03
C2A-C3A	0.31±0.03	0.31±0.03	0.31±0.03	0.33±0.03	0.36±0.03	0.38±0.03
C3A-C4A	0.19±0.03	0.20±0.03	0.19±0.02	0.21±0.03	0.24±0.03	0.25±0.04
GL2-C1B	0.39±0.03	0.41±0.03	0.40±0.03	0.41±0.03	0.43±0.03	0.44±0.03
C1B-C2B	0.38±0.02	0.39±0.02	0.38±0.03	0.40±0.02	0.43±0.03	0.44±0.02
C2B-C3B	0.31±0.02	0.32±0.03	0.29±0.03	0.32±0.03	0.36±0.03	0.37±0.03
C3B-C4B	0.19±0.03	0.21±0.03	0.17±0.02	0.21±0.03	0.23±0.03	0.24±0.04
Average	0.25±0.01	0.26±0.01	0.25±0.01	0.26±0.01	0.29±0.01	0.29±0.01